Flow Past Two-Dimensional Ribbon Parachute Models

Hiroshi Higuchi* and Fumiyuki Takahashi†
University of Minnesota, Minneapolis, Minnesota

Aerodynamic characteristics of two-dimensional, slotted bluff bodies are experimentally investigated. The models consist of a series of thin flat plates arranged to form flat and curved geometries. Flow visualizations, base pressure measurements, mean velocity vector measurements, and drag force measurements are conducted to analyze the effects of spacing ratio (i.e., porosity), curvature, and a center opening (i.e., vent). Low-porosity model configurations produced stable near-wake patterns with enhanced vortex sheddings downstream. Model curvature reduced drag forces and weakened the vortex sheddings. Stabilizing effect of curvature on the near-wake patterns was also found. A vent combined with large model curvature was found to reduce drag force significantly as well as suppress the vortex sheddings among models with equivalent porosity.

WAKE downstream of slotted bluff bodies exhibits complex structures caused by vortex sheddings of the overall wake and interactions of high-speed jets through multiple gaps. Clear understanding of the flowfields behind such bluff bodies is of practical importance in relation to such problems as wake-canopy interactions behind ribbon parachutes[1] and vibrations of heat-exchanger tubes and other structures.[2] At very large spacings between the bodies, the wakes behind individual bluff bodies have been known to behave more or less independently, whereas at small spacings, the overall wake behind a row of multiple bodies resembles that behind a single bluff body with regular vortex sheddings. At intermediate spacings, however, the wakes behind individual elements start interacting with each other to form irregular flow patterns.[3,4] Furthermore, the patterns may change spontaneously or they can be changed into different configurations by perturbing the incoming stream. Generally, several flow patterns are possible for a given body configuration, and this irregular near-wake pattern appears to have a large influence on the overall wake formation.

Several researchers in the past[3,5-7] have investigated the flowfield past a row of a small number of bluff bodies aligned normal to the freestream. These works showed that either stable or bistable pressure distribution existed depending on the model configurations. The longitudinal curvature of two-dimensional grid models, consisting of a large number of elements,[4] was found to have a stabilizing effect on the immediate downstream flow pattern by forcing the incoming flow toward the center. According to the recent study by Hayashi et al.,[8] the curvature of concave solid bodies simulating two-dimensional parachute models affected the size of the wake and the drag force. It has also been pointed out[9] that slots located near the center of the elliptic two-dimensional solid bodies reduced the drag force effectively. Besides the curvature and porosity, the vent placed on the center of the concave body should be studied as an effective means of controlling the drag. Roberts[10] measured pressure distributions on a family of porous slotted disks and found the slot arrangement to be an important factor in determining the drag coefficient as well as the porosity of the model.

Detailed studies, however, have yet to be conducted to examine the flow structure downstream of bluff bodies consisting of a large number of flat plate elements. A practical example of such flow can be seen behind ribbon parachutes. In addition to the complex wake structure caused by the large number of elements arranged on a concave surface, a vent as positioned at the apex of the parachute canopies adds further complexity to the wake formation. In addition, although several major parameters were found to govern the aerodynamic characteristics of concave bluff bodies, their combined effects have not been analyzed sufficiently. It is, therefore, the objective of the present experimental investigation to parametrically study the effects of the porosity, curvature, and vent on the flow structure and drag force, and the stability of the wake pattern. This experimental investigation is focused on the aerodynamics of two-dimensional slotted bluff bodies, but it is hoped that the findings will help one analyze the basic structures of flow past more general, concave, slotted bluff bodies.

Experimental Procedure

Two low-speed wind tunnels, one an open-return type and the other a closed-return type, were utilized. The major portion of the experiment was carried out in the open-return wind tunnel. The test section of this wind tunnel is 1.83 m long with a 30.5×43.2 cm cross section. The contraction ratio is 9:1 and the inlet is equipped with a honeycomb followed by two screens. The exhaust housing was modified to achieve a smooth freestream of nominal 6 m/s. A hot-wire anemometer survey showed a turbulence level of 0.26%.

A low-speed, closed-return wind tunnel was used for the drag force measurements with a strain-gage drag balance. The closed test section used is 1.5 m long and the cross section measures 137×97 cm. The mean turbulence level in the test section was found to be approximately 0.8%.

The model configurations are shown schematically in Fig. 1. The model's overall width, denoted by W, was fixed at 8 cm. The 12 models consisted of a series of thin flat plates arranged to form models of two different curvatures and flat models. Each flat-plate element was made of a titanium alloy and measured 5 mm high, 1.2 mm thick, and 305 mm long. The spacing s between plates was varied between 0.5 and 0.25 of the plate height h. The models with a vent were produced by simply removing a plate at the center of each model. The surface porosity, evaluated using the total model surface area, ranged from 18.75 to 37.5%, and the projected porosity varied from 18.75 to 39.42%. In the open-return wind tunnel, these models were tested at an upstream velocity of nominal 6 m/s. The Reynolds number based on the model's overall width and the freestream velocity past the shoulder of the models was 38,000. In order to establish a two-dimensional flowfield, 2.54-mm thick end plates with a tapered leading

Presented as Paper 88-2524 at the AIAA 6th Applied Aerodynamics Conference, Williamsburg, VA, June 6-8, 1988; received June 23, 1988; revision received Nov. 29, 1988.

*Department of Aerospace Engineering and Mechanics; currently at St. Anthony Falls Hydraulic Laboratory. Senior Member AIAA.

†Graduate Research Assistant, Department of Aerospace Engineering and Mechanics; currently at Nomura Research Institute and Nomura Computer Systems, Tokyo, Japan. Member AIAA.

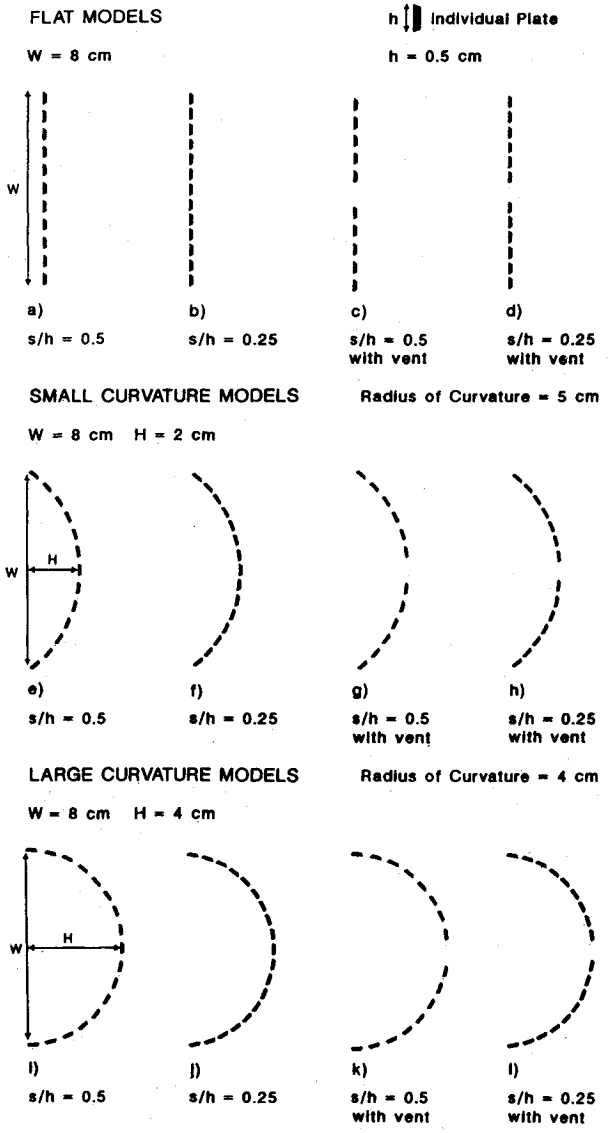

Fig. 1 Model configurations.

edge were placed at 2.54 cm from the wind-tunnel side walls, covering 110 mm upstream and 330 mm downstream of the model's leading edge. The blockage ratio of the model and end-plate assembly of the maximum-solidity flat model was approximately 19.4% in the open-return wind tunnel. The axial pressure distributions in the freestream with the model in place are reported in Ref. 11. The blockage ratio in the closed-return tunnel was substantially reduced, as discussed later.

An aluminum tubing of 0.79 mm in diameter was attached at the center of the leeside of the individual plate element during the base pressure measurements using a Datametrics-Dresser 10-mm Hg-range electronic pressure transducer. Throughout the measurements, the time-dependent nature of the flow due to the spontaneous change in the wake pattern was monitored with the inclined multiple manometer and smoke flow-visualization technique.

The wake formations downstream of the models were examined with a smoke flow-visualization technique using a Rosco 1500 fog generator. With a streamlined nozzle placed at the inlet of the tunnel, a relatively thin sheet of smooth smoke was produced in the test section. The thickness and height of the smoke at the empty test section were measured to be about 1.2 and 11 cm, respectively. The smoke flow past the model was illuminated by an electronic flash at approximately 1/20,500 s duration. The two-dimensionality of the wake was verified by the flow visualizations.

The time-averaged velocity vector field downstream of the models was surveyed by a split-film probe (TSI 1288) operated by a pair of DISA-type 55M10 constant-temperature anemometers. The vortex-shedding frequency was determined with a HP digital-spectrum analyzer. The calibration procedure of the split-film sensors was similar to that reported in Ref. 12. The calibration of the probe as well as the uncertainty analysis of the mean velocity measurements are discussed in Ref. 11.

In order to minimize blockage effects on the drag measurements, the test models were subsequently installed in the larger test section of the closed-return wind tunnel. Aluminum end plates 2.54 mm thick and 50 cm high covered 20 cm upstream and 50 cm downstream of the models. The models were supported by low-friction slide bearings, and the aerodynamic drag on the test models was measured by a strain gage attached to the model support. The maximum blockage ratio of the entire model assembly was estimated to be 4.6%. Each of the model configurations was tested at the incoming freestream speeds of 9 and 12 m/s, but the normalized drag coefficients were almost identical for two freestream velocities tested. The corresponding Reynolds numbers were about 50,000 and 66,000, respectively.

Results

Flow Visualizations and Pressure Distributions

Wake patterns were monitored by flow visualization and multiple manometers, as mentioned earlier, and corresponding pressure distributions were recorded. In order to study nonunique flow patterns for a given model configuration, the wind tunnel was stopped and restarted several times after the first observation. To study the flow stability once a certain wake pattern was established, the incoming flow was momentarily perturbed. For this purpose, the external disturbance was applied by inserting a porous metal screen into the upcoming freestream for about 10 s. Thereafter, additional external disturbances were introduced as appropriate.

Flow visualization photographs of wake formations are presented together with pressure distributions on the leeward side of the models. Results of the pressure-distribution measurements are given in the plots of normalized pressure coefficients $C_p/C_{p_{\text{mean}}}$ vs plate locations as well as the averaged values of the mean pressure, $C_{p_{\text{mean}}}$. The base pressure on each plate was found in an earlier test to be almost uniform. In the calculation of a pressure coefficient C_p, static and dynamic pressure were referenced to the freestream past the model. The average pressure coefficients given in the pressure-distribution plots, therefore, represent blockage-corrected values for freestream acceleration due to the body blockage. The effect of body and wake blockages on the $C_{p_{\text{mean}}}$ values is discussed in Ref. 11. The results are presented next in the order of flat models, small curvature models, and large curvature models following the sequence shown in Fig. 1.

Flat Models

***s/h* = 0.5**–Two predominant wake patterns were found; both had large recirculating zones starting at the central plate. One of the two patterns is represented in Fig. 2. Figures 2a and 2b are smoke flow-visualization photographs of the overall wake formation and near-wake pattern. The presence of differently sized recirculating zones is seen behind individual plates. Furthermore, these recirculating zones were arranged almost symmetrically with respect to the center of the model. A large recirculation zone, located behind the central plate of the model, dominated the others both in size and pressure. The pressure pattern is shown in Fig. 2c. Comparison between Figs. 2b and 2c shows that a small $C_p/C_{p_{\text{mean}}}$ (a low negative pressure) corresponds to a large recirculating zone behind that particular plate, and a large $C_p/C_{p_{\text{mean}}}$ conversely to a small recirculation zone. For example, the large recirculation region near the center is clearly seen both in Figs. 2b and 2c. The wake pattern of Figs. 2a–c was bistable. The gap flows on both sides of the second plate from the top flip-flopped, pro-

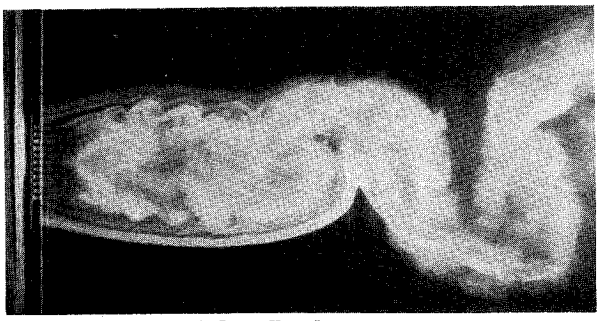

a) Overall wake pattern

b) Near-wake pattern

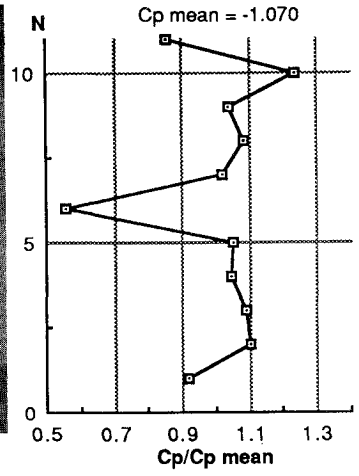

c) Base pressure distribution

Fig. 2 Flat model, $s/h = 0.5$.

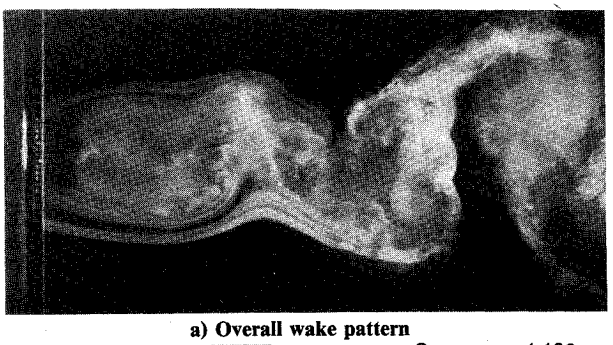

a) Overall wake pattern

b) Near-wake pattern

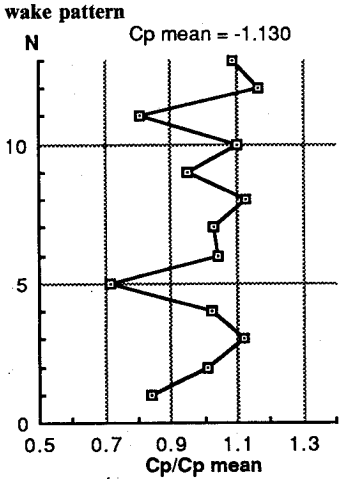

c) Base pressure distribution

Fig. 3 Flat model, $s/h = 0.25$.

ducing alternating recirculating zones with a time period of about 1 s. Similarly, recirculating zones behind the two outermost plates flip-flopped in their sizes. In spite of these transient motions, the time-averaged pressure distributions of these two profiles indicate almost symmetric near-wake configurations. Note that the smoke flow-visualization photograph (Fig. 2b) clearly shows two streets of small vortices along the shear layers emerging from both edges of the model. These two initial wake patterns were easily disturbed and, most frequently, resulted in another asymmetric pattern with the large separation bubble shifting from the center of the next one down. In spite of different near-wake patterns, overall wake fields were similar among all cases, and the value of $C_{p\text{-mean}}$ remained nearly constant.

$s/h = 0.25$–Only a single wake pattern was observed as shown in Fig. 3. This wake pattern was very stable in spite of its slight asymmetry, and even repeated external disturbances had little influence. The vortex-shedding motion was more vigorous than in the large-spacing ratio case, and the wake rollup began closer to the model. Compared to the larger-spacing case in Fig. 2, this profile exhibited small recirculating zones merging together toward the center, instead of a large recirculating zone at the center.

$s/h = 0.5$ with Vent–This model configuration gave rise to a number of asymmetric near-wake patterns accompanied by a deflected center jet through the vent. A wake pattern, as presented in Fig. 4a, which had a downward-deflected jet through the vent, appeared most frequently after the tunnel startup. The pressure profile in Fig. 4c is highly skewed because of the deflected center jet. A large recirculating zone existed invariably on the unbiased side of the vent flow. The vortex sheddings in the far wake became weaker with the introduction of the vent jet compared to those without a vent (compare Fig. 4a with Fig. 2a). The external disturbances applied to this flow pattern generated numerous near-wake patterns with different directions for the center jet deflections.

$s/h = 0.25$ with Vent–Only one near-wake pattern was initially produced, although external disturbances transformed

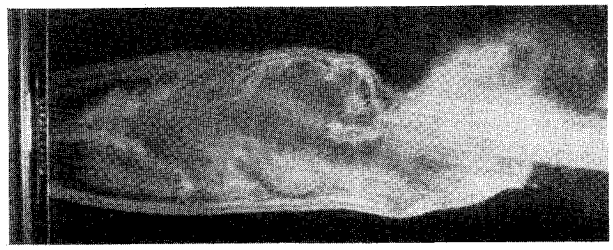

a) Overall wake pattern, $s/h = 0.5$

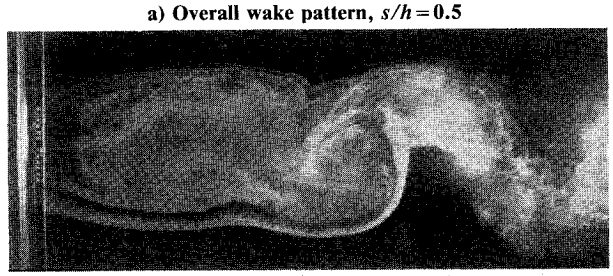

b) Overall wake pattern, $s/h = 0.25$

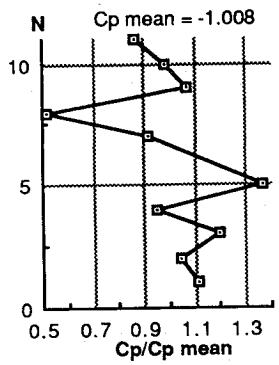

c) Base pressure distribution, $s/h = 0.5$

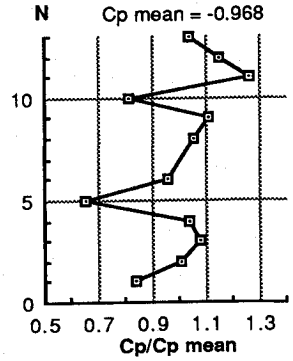

d) Base pressure distribution, $s/h = 0.25$

Fig 4 Flat models with vent.

this pattern into various near-wake patterns. In this flow configuration, as shown in Figs. 4b and 4d, the center jet was deflected upward and a large recirculating zone occupied most of the downstream wake. Figure 5 depicts the detailed motion of the asymmetric wake configuration of Fig. 4b; it shows the rollup of the large vortices as they are convected downstream. Also, a relatively stationary near-wake pattern can be noted.

Small Curvature Models

$s/h = 0.5$–This small curvature model resulted in a reduced number of near-wake patterns.[11] As was the case in the flat model with the same spacing ratio, a large recirculating zone was always present at the center of the model at the beginning. The initial flow patterns were easily changed into irregular patterns by external disturbances. All of these wake patterns had predominantly large separation bubbles positioned at one plate off the center, but these profiles could be brought back to the original profiles by additional external disturbances. In spite of several different near-wake patterns, all of the overall wake-formation patterns were found to be similar.

$s/h = 0.25$–At the small-spacing ratio with small curvature, only a single wake pattern with a large recirculating zone at the center was found intially. As in the flat-model case, external disturbance had no influence on the flow. The far wake exhibited distinct vortex sheddings, but in comparison to the wake pattern of the flat model, the wake rollup process was slightly delayed.[11]

$s/h = 0.5$ with Vent–Three initial wake patterns emerged, with the center jet deflected upward or downward, or undeflected. External disturbances to the incoming freestream caused the flow to vary among these patterns and also produced additional profiles. These flow patterns, however, eventually resulted in the initial deflected pattern. The different near-wake patterns significantly affected the far wake. For example, Fig. 6a shows a near wake with an undeflected jet and medium-size recirculating zones, one on each side of the vent. Further downstream, outer shear layers formed two rows of alternating vortex streets. In another wake pattern found with the undeflected jet, the vortex sheddings were further delayed. When the jet through the vent was deflected, on the other hand, it produced either a symmetric far-wake pattern without vortex shedding, or an asymmetric wake pattern with a vortex street only on the deflected side of the wake. Flow patterns and pressure distributions for these cases can be found in Ref. 11.

$s/h = 0.25$ with Vent–Asymmetric wake patterns were always found at this small-spacing ratio with vent. The profile in Fig. 6b was the pattern that emerged initially. The vent flow of this pattern is seen deflected upward; a large recirculating zone appears on the unbiased side of the wake, terminated by the large streamline curvature. External disturbances to this flow introduced additional patterns, with the center jet deflected upward or downward without preference as to its direction. The overall wake shapes of all these flow patterns were essentially the same despite the different directions of the jet deflection.

Large Curvature Models

$s/h = 0.5$–Figure 7a shows the typical overall wake pattern for this model configuration, where the symmetric wake boundaries lack any marked vortex rollup motion. No essential difference was found in the shapes of the overall wake among different near-wake patterns. Only the near-wake pattern shown in Fig. 7b was observed initially. A large recirculating

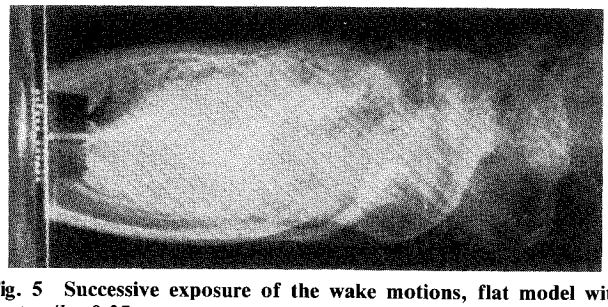

Fig. 5 Successive exposure of the wake motions, flat model with vent, $s/h = 0.25$.

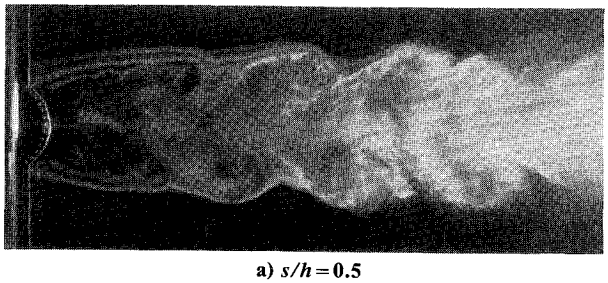

a) $s/h = 0.5$

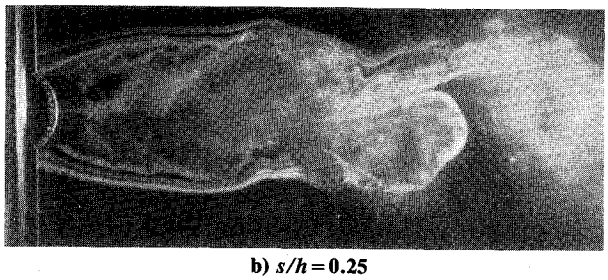

b) $s/h = 0.25$

Fig. 6 Overall wake patterns for the small curvature models with vent.

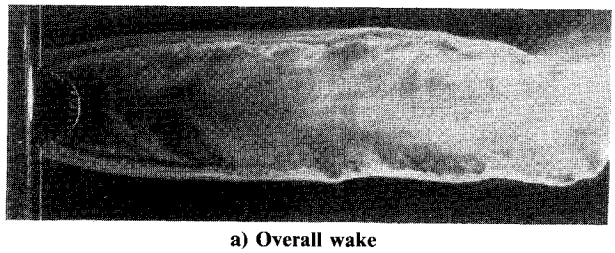

a) Overall wake

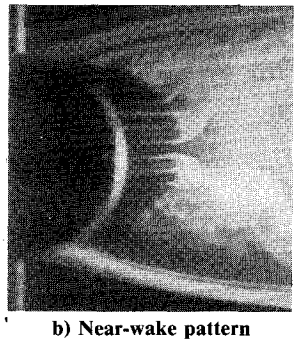

b) Near-wake pattern

c) Near-wake pattern

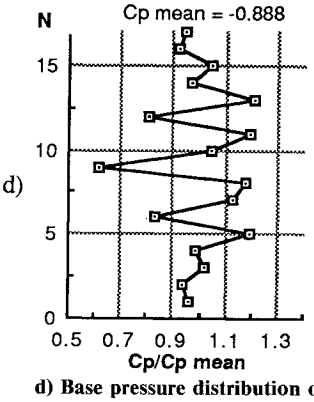

d)

d) Base pressure distribution of near-wake pattern, (shown in b)

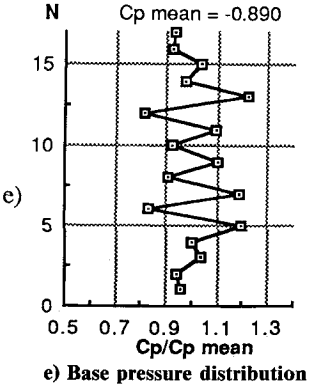

e)

e) Base pressure distribution of near-wake pattern, (shown in c)

Fig. 7 Large curvature model, $s/h = 0.5$.

zone was located at the center, similar to the flat-model case in Fig. 2b. The gap flows near the edges of the model make large angles with respect to the incoming freestream, but overall wake size is smaller with the curvature. A nearly symmetric pressure distribution as shown in Fig. 7d corresponds to this near-wake pattern.

When the incoming flow was externally disturbed, this profile changed into two bistable profiles. A large recirculation zone was located off center, and shifted its position between two plates near the central plate at the time interval of about 3 s. About 3 to 5 min later, however, these bistable wake patterns transformed themselves into a new stable pattern (Fig. 7c). In contrast to the profile in Fig. 7b, which was also symmetric, a small recirculating zone was at the center. This profile could be brought back to the original wake pattern of Fig. 7b by repeated external disturbances.

The $C_{p_{mean}}$ of the leeward side of the model was almost constant, regardless of the different near-wake patterns, and this is evident between the present two flow patterns (compare Figs. 7d and 7e).

$s/h = 0.25$–At a small-spacing ratio of $s/h = 0.25$, only one wake pattern was found even with external disturbances. As shown in Fig. 8, recirculating zones were distributed almost symmetrically with a large recirculating zone at the center. In comparison with the relatively smooth streamlines of the outerwake boundary at the large-spacing ratio (Fig. 7a), a vigorous flow-entrainment process was observed with distinct vortex sheddings (Fig. 8a).

$s/h = 0.5$ with Vent–The profile shown in Figs. 9a and 9c was the only wake pattern that appeared intially. These figures show the unbiased center jet surrounded by two equally small bubbles. The overall wake shape was essentially unchanged with the presence of the vent. This profile had a nearly symmetric pressure distribution. Although the profile persisted for a long time in most cases, some asymmetric patterns occurred naturally or by external disturbances. The resulting flow pattern with the biased jet through the vent was stable, and no effect of flow disturbance was observed later. There was no preference in the directions of the bias. In the far-wake region, vortices started to roll up gradually downstream of the deflected side of the center flow, while formation of a vortex street was further delayed on the opposite side of the wake.[11]

$s/h = 0.25$ with Vent–Two types of asymmetric wake profiles were found, and they alternated between one another once, upstream disturbances were applied. Figs. 9b and 9d show, respectively, the wake formation and pressure distribution of one of these two patterns, which had an upward biased center jet. The deflected jet through the vent suppressed the large-wake interactions that were seen at the same spacing ratio without vent, producing a fairly symmetric overall wake shape. In addition, unlike the large-spacing case with the same curvature, the deflected jet did not form any detectable vortex rollup. Compared to the flat model with vent (see Fig. 4b), large curvature produced less asymmetric wake shape with reduced vent flow deflection.

Velocity Profiles

Mean velocity vector distributions in the near-wake regions behind each model configuration were measured using the split-film anemometer. The magnitude of velocity was normalized by the local freestream velocity outside the wake, based on axial static pressure measurements along the tunnel wall. The uncertainty in the magnitude of velocity was estimated to be at most $\pm 6\%$ of the freestream velocity and in the angle to be ± 3 deg.[11] The overall profiles will be shown in detail for one representative flow pattern, and the velocity profiles for four other model configurations will be compared at two model-heights downstream ($X/W = 2$).

The overall velocity distributions in the wake of the small curvature model at $s/h = 0.25$ with vent are presented in Fig. 10. The wake pattern corresponds to that shown in Fig. 6b. This velocity profile clearly shows the formation of the large

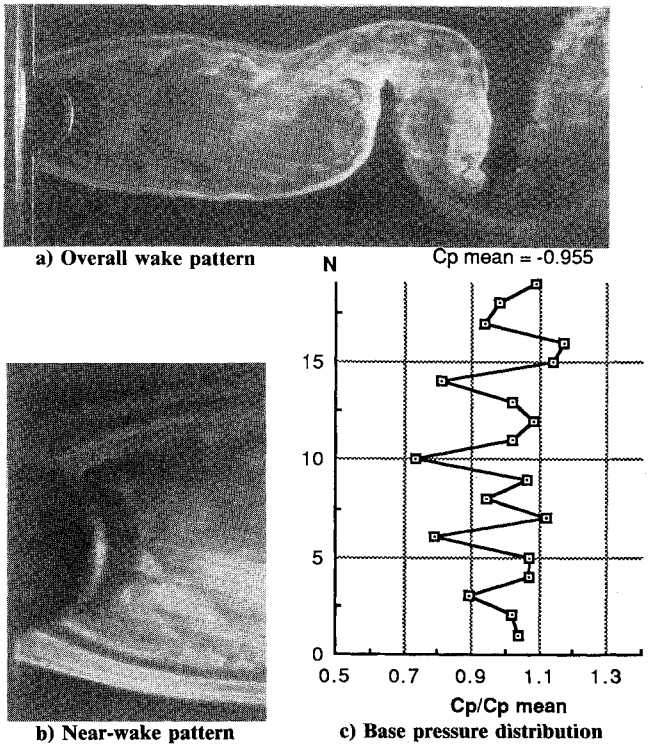

Fig. 8 Large curvature model, $s/h = 0.25$.

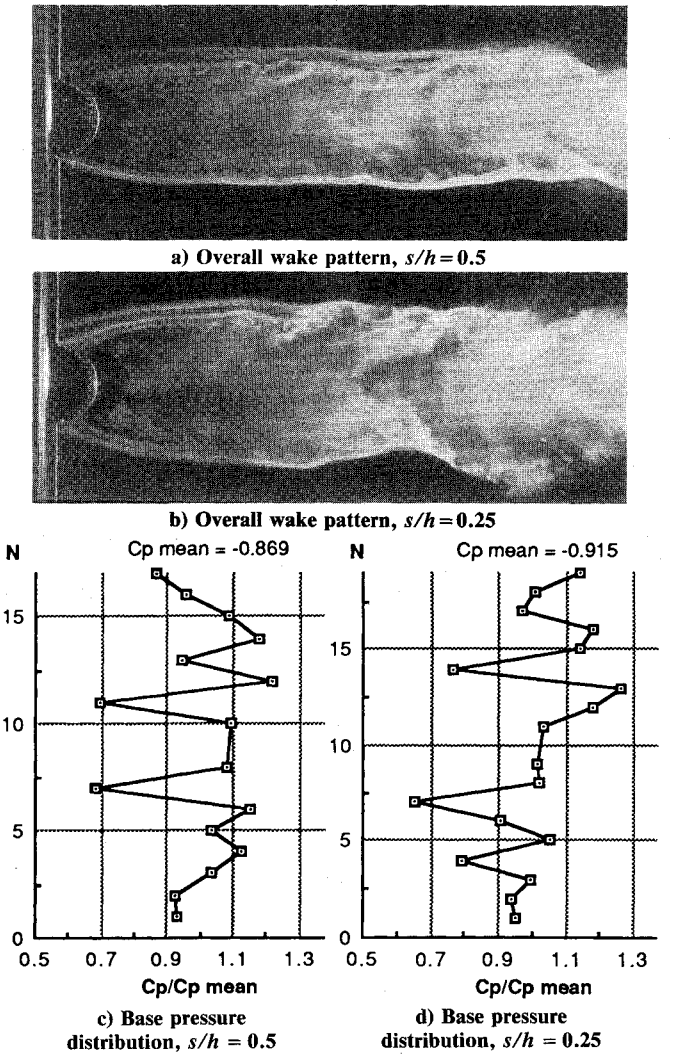

Fig. 9 Large curvature models with vent.

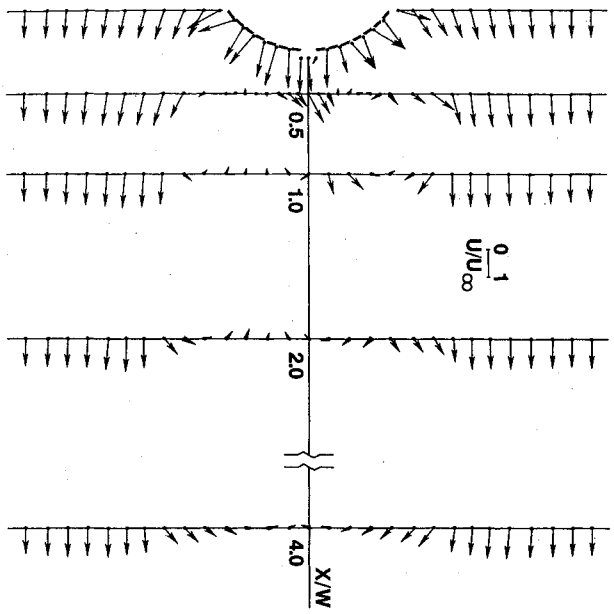

Fig. 10 Overall velocity vector profile behind small curvature model with vent, $s/h = 0.25$.

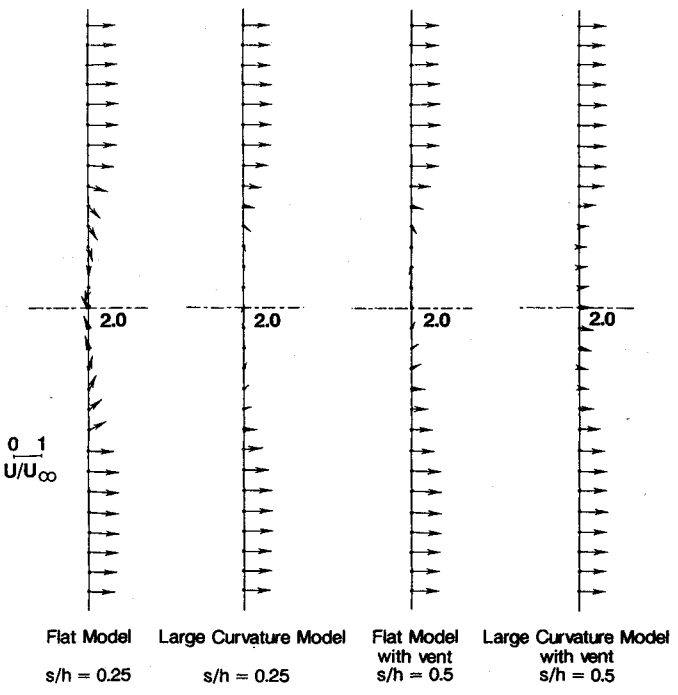

Fig. 11 Velocity profiles at $X/W = 2.0$

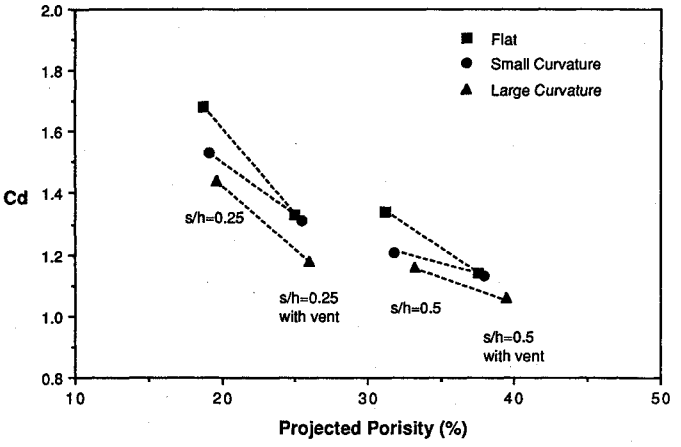

Fig. 12 Drag coefficients of the models.

recirculating zone extending downstream of the flow. The high-speed center jet is seen largely deflected in the opposite direction of the large recirculating zone. Negative flow velocity at $X/W = 0.5$ on the deflected side of the jet through the vent is evidence of a small recirculation zone immediately downstream of the model.

Velocity vector profiles are compared between a flat model and a large curvature model in Figs. 11a and 11b. The flow patterns corresponding to these profiles were shown earlier in Figs. 3a and 8a, respectively. The wake boundaries behind the flat model appear to be still expanding at this axial station, with distinct reversed flow regions near the center of the wake. The velocity profile behind the curved model indicates a much smaller reversed flow region at this station.

Figures 11c and 11d compare the effect of the vent on the velocity distributions of the flat and curved models at the spacing ratio $s/h = 0.5$. These profiles correspond to the profiles of Figs. 4a and 9a, respectively. The velocity profile of the flat model shows a large reversed-flow zone on the undeflected side of the vent flow. On the other hand, the velocity field behind the curved model shows a symmetric profile with an undeflected jet into the center of the wake, and no reversed flow region is observed.

The wake vortex sheddings were monitored concurrent with the velocity profile measurements. The Strouhal number based on the freestream velocity past the models measured at $X/W = 9$ behind the models varied from 0.17 to 0.18 for the models without vent. The shedding frequency did not depend strongly on the model porosity, but it tended to decrease with increasing curvature, particularly between flat and small curvature models, corresponding roughly to the observed wake widths.

For the models with vent, the regular vortex sheddings were weakened for the case of $s/h = 0.5$ (see, for example, Figs. 4a and 9a). High-frequency instability waves seen on the wake boundaries immediately downstream of some models with or without vent dissipated prior to the regular vortex rollup downstream (see Figs. 2a and 8a).

Drag Measurements

Drag force was measured by the drag balance method in the closed-return wind tunnel. The blockage effect on the drag measurements was estimated using the formula of Allen and Vincenti.[13] The ratio between uncorrected and corrected drag coefficient ranged from 0.96 to 0.98, depending on the model configurations, and was thereby regarded to be unity.

Figure 12 shows the drag coefficient vs porosity plot, where the drag coefficient C_d is based on the projected overall frontal area of the model. The increasing porosity of the model reduced the drag as expected. However, the drag force did not decrease monotonically with the porosity, but depended on the model configuration. For example, the values of C_d increased in spite of a porosity increase when the model configuration was changed from the large curvature model at $s/h = 0.25$ with vent to the flat model at $s/h = 0.5$. The effects of curvature, vent, and spacing ratio (porosity) on the value of the drag force are seen in the figure. The curvature and vent were found to decrease the drag force effectively. As for the models without vent, the reduction of the drag was significant when the curvature was applied to the flat model, keeping the porosity nearly constant. On the other hand, in the case of the models with vent, adding further curvature to the small curvature models caused a large drop in C_d, but curvature applied to the flat models resulted in little change in C_d. The figure also shows that the vent on the smaller-spacing ratio model reduced C_d values more effectively than its counterpart at the larger-spacing ratio.

Discussion

Effects of Spacing Ratio

Different model spacing ratios between $s/h = 0.5$ and 0.25 significantly affected the aerodynamic characteristics of the models. In general, the reduction in spacing ratio or a decrease in model porosity caused the increase in drag as shown in Fig. 12. The velocity profiles were consistent with the results of the drag measurements. The drag coefficients of the present flat-model configurations which consisted of 11 or 13 plate elements, are compared with those of four-plate row models in Fig. 13. The results of the four-plate model by Hayashi et al.[3] showed two distinctly different drag values at a fixed porosity based on different near-wake patterns, whereas no such large deviations in the values of C_d were recorded for the present models. Although an individual element may have experienced a large variation in the base pressure both on flat and curved models, the base pressure averaged among a large number of elements over an entire model ($C_{p_{\text{mean}}}$) remained almost constant for a given model configuration, regardless of the various flow patterns. Note, for example, a negligible difference in $C_{p_{\text{mean}}}$ values in Figs. 7d and 7e. In general, the drag variation with the model porosity showed a similar trend among different flat models with various opening geometries, including that of perforated plates.[14] However, the drag coefficients of the present two flat models without vent were higher than those of the perforated plates and four-plate models at the same porosities. Additional drag measurements on the present flat models were made at the same fixed-spacing ratios, but by varying the number of plates incrementally from 4 to 13. Normalized drag coefficient increased with the number of plates in spite of a slight increase in model porosity, indicating that the drag was affected by the detailed wake interactions downstream of individual slots. This was consistent with flow visualizations that showed wider near-wake recirculating zones behind the present 13 plates ($s/h = 0.25$) and 11 plates ($s/h = 0.5$) than those behind the four-plate model that showed wider near-wake recirculating zones behind the present 13 plates ($s/h = 0.25$) and 11 plates ($s/h = 0.5$) than those behind the four-plate model. (The detail wake pattern behind the perforated plates is not available in Ref. 14. It is yet to be seen whether perforated plates should behave as a limiting case of flat plate models.)

With regard to the overall wake formation, reducing the spacing ratio, i.e., decreasing the model porosity, formed more distinct shear layers on the wake boundaries with reduced momentum in the wake. The enhanced entrainment by these two outer shear layers intensified the overall vortex sheddings. (Compare Figs. 2a and 3a for a flat-plate model, and Figs. 7a and 8a for the large curvature models.) These effects were in accordance with Castro's[14] observation that indicated two distinct flow regimes downstream of the perforated plate depending on the model porosity: one corresponding to the low value porosities, where the vortex streets dominated the wake, and the other at higher porosities characterized by a fully turbulent flow. With the addition of a vent, the far-wake patterns of the small-spacing ratio models generally became more asymmetric due to the larger deflection of the center jet, but as was the case without vent, the vortex sheddings of these asymmetric wake formations were enhanced with the small-spacing ratio (for example, compare Figs. 4a and 4b or 5).

Near-wake flow patterns, while being irregular, appeared to be stabilized by the reduced spacing ratio. One could argue that, between the two spacing ratios presently studied, the jets through narrower gaps were relatively further separated from one another compared to the large-spacing ratio case and that this resulted in reduced interaction among jets. The stabilizing effect of the smaller-spacing ratio was distinctly observable for the models without vent. A number of various near-wake flow patterns emerged at the large-spacing ratio. On the other hand, at the small-spacing ratio, only a single near-wake pattern resulted from each of the three different curvature

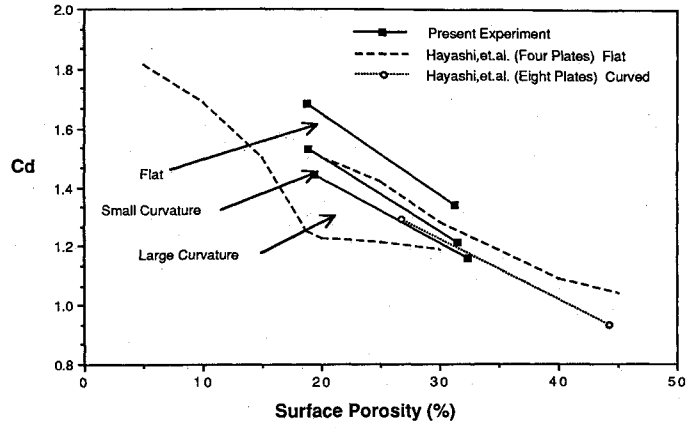

Fig. 13 Effect of curvature and porosity on drag.

models, and in addition, these flow patterns (see, for example, Figs. 3 and 8) were very stable and immune to external disturbances. The flip-flopping phenomenon observed behind the large curvature and flat models at the large-spacing ratio did not occur when the spacing ratio was halved. At the small-spacing ratio, smaller recirculating zones were found at the leeward side of the model elements, and the variation of $C_p/C_{p_{\text{mean}}}$ values among individual plates decreased.

The effect of the spacing ratio on the near-wake patterns was less clear for the models with vent due to the jet deflections. Although fewer initial wake patterns were observed compared to those without vent, the reduction in the number of the flow patterns was less marked at the small-spacing ratio, and these near-wake patterns could be easily perturbed by external disturbances; this was particularly true for the flat models. Nevertheless, the overall effect was that fewer numbers of the near-wake patterns appeared compared to the large-spacing ratio case.

Effects of Curvature

The aerodynamic characteristics of the two-dimensional slotted models changed considerably as the model curvature was increased from the flat to large curvature configuration. The major effects included drag reduction, delayed vortex shedding, and near-wake stabilization (namely, increased resistance to flow perturbation and reduction in the number of near-wake patterns). These effects of curvature for the models without vent are discussed first, followed by a discussion of the models with vent.

The effect of the model curvature on the drag force was notable. Figure 13 shows the significant decrease in C_d caused by the model curvature. Here, the surface porosity was used so that Hayashi et al.'s C_d values of semicircular, thick, eight-element models[9] can be included for comparison, while for the present models, the difference between the surface porosity and the projected porosity was almost negligible. (Two curves for Hayashi et al. flat models[3] correspond to two wake patterns observed.) The wake velocity profiles showed that the axial momentum of the flow increased with curvature (Figs. 11a and 11b). It appears that by forcing the incoming flow toward the center of the slotted models, the model curvature increased the momentum inside the wake, which is reflected in the result of the drag force measurements. It is of interest to contrast this curvature effect with that on the solid model. An increase in the C_d values of the circular-arc solid models with curvature up to $H/W = 0.4$ was reported.[8] The present experiment carried out for the slotted models, on the other hand, indicates the opposite trend. In the solid model, a near stagnant flow zone exists inside or slightly ahead of the plane of the model leading edge, depending on the model curvature. The flow-visualizaton photographs of Hayashi et al.[8] indicate widening of the near-wake as the model curvature increases. For the present slotted model, on the other hand, the incoming stream flowed smoothly toward the center of the concave sur-

face, injecting more jet momentum through gaps at larger curvature.

Associated with the increased momentum in the wake, the shear layers at the wake boundaries became weak and the formations of the vortex streets were delayed. The interaction between two outer shear layers on the wake boundaries was weakened by increasing the model curvature. Therefore, large wake oscillations observed far downstream of the flat model diminished with the increased curvature (compare Fig. 2a with Fig. 7a).

At the immediate downstream of the models without vent, the large model curvature caused the near-wake patterns to be more symmetric, especially at the small-spacing ratio. Moreover, the curvature produced a predominantly large recirculating zone at the center of the near wake. These are evidenced in the flow visualizations (Figs. 7b and 8b) behind the large curvature models. In comparison, near-wake formations were less symmetric at small curvature, while the large recirculating zone was still positioned at the center. On the other hand, behind the flat model at the small-spacing ratio, the large recirculating zone was no longer present in the wake formtion. Instead, medium-size bubbles were observed near the center of the model (Fig. 3b). The flat model flow pattern of the large-spacing ratio (Fig. 2b) exhibited near-wake formations similar to those in the flow behind the small curvature models. Furthermore, these flow patterns of the large curvature and flat models were more easily disturbed than the flow patterns of the large curvature model. The reduced curvature moved the large recirculating region off the center, and as a result, asymmetric flow patterns appeared.

At the large-spacing ratio, the large curvature models produced fewer irregular near-wake patterns than the flat model. A similar effect has been observed in the experiment conducted for flat and curved models with a row of a large number of plates (up to 26) extending over the test section,[4] although the boundary conditions of that experiment were somewhat different from those of the present study. The model curvature directed the incoming flow toward the center of the model and induced a symmetric wake pattern, making the near-wake patterns more resistant to external disturbances.

The models with vent showed curvature effects similar to those of the models without vent discussed previously. The increased model curvature reduced the C_d values, as was the case of models without vent, although the drag reductions from the small to large curavture models were larger than those for the models without vent (Fig. 12). This difference is attributed to the strength of the vent jet as discussed later. As was the case in the models without vent, the increase in the model curvature led to a substantially reduced number of near-wake patterns. Increased model curvature evidently increased the momentum of the jet through the vent as seen, for example, in Figs. 11c and 11d. For the small curvature and flat models, the near-wake patterns were more asymmetric due to the center jet deflection. For the small curvature model at large spacing, the undeflected center jet turned into the deflected patterns by itself and formed asymmetric near-wake patterns. Meanwhile, at the small-spacing ratio, only a deflected center jet existed regardless of the model curvature. The deflection angle of the center jet became smaller as the model curvature was increased (compare the overall wake formations in Figs. 4b and 9b). Thus, for the models with vent, the model curvature was found to reduce the center jet deflection and, consequently, more symmetric wake patterns appeared.

Effects of Vent

An opening located at the center of the model was found to play an important role in drag and wake formation for all of the configurations presently investigated.

For comparable model porosities, the vent at the center of the model reduced the drag force more effectively than the increased spacing ratio. Moreover, a combination of the vent and large model curvature resulted in the lowest C_d values per given porosity in both of the two spacing ratios. The velocity profile plots (Fig. 11d) and flow-visualization photographs (Fig. 9a) behind large curvature models show a high-speed jet through the vents injected into the downstream wakes. Meanwhile, jets from the vents of small curvature and flat models were, in most cases, highly deflected (see Figs. 6a, 6b, and 10 for the small curvature model and Fig. 4a, 4b, and 11c for the flat model). At the same time, as the deflection of the jet became larger, the reversed flow region grew on the opposite side of the jet deflection. Thus, the contribution of the momentum of the jets to drag reduction was less significant, and the amount of the C_d drop between flat and small curvature models was much less than that between large and small curvature models as indicated in Fig. 12.

The influence of the vent jet on the shape of the overall wake formation depended on the curvature and the spacing ratio. The vent on the small curvature, large-spacing ratio model resulted in more complex wake structures than the case without vent, as shown in Figs. 6a and 6b. The vent located in the flat and small curvature models with the small-spacing ratio caused wider wakes, accompanied by large recirculating zones positioned on the undeflected side of the center jets (see Figs. 4b and 6b). On the other hand, since the large curvature, large-spacing ratio model without vent did not show any clear vortex sheddings (Fig. 7a), an addition of the vent had little influence on the vortex formations (Fig. 9a). With large curvature at a small-spacing ratio, the vortex street formations without vent in Fig. 8a were suppressed by the jet introduced into the wake, and relatively smooth wake boundary streamlines appeared as shown in Fig. 9b. It appears that, for the large curvature model, the large momentum jet through the vent suppressed the formation of regular vortex sheddings by obstructing the interaction of the two shear layers from the model shoulders. Even for the cases with small-spacing ratio in which some vortex formations could be measured, the variation of vortex-shedding frequency was not correlated to the model curvature unlike the models without vent.

The present study, therefore, suggests that the effect of detailed model geometry must be taken into account in examining the aerodynamic characteristics of the slotted model. If the number of plate elements becomes small, the number and arrangement of the elements become important. (This is in contrast to the earlier study[4] involving grid models in confined airstreams with large numbers of elements, in which the pressure drop coefficients under the given porosities were found somewhat insensitive to the particular geometries and near-wake patterns.) The dependency of the drag of flat models on the number of elements had been mentioned earlier. As another example, concave models can be made of either an odd or even number of plate elements, keeping the porosity of the model the same. An odd-number element model has a plate located at the apex of the model, as is the case in the present study, whereas a model that consists of even-number elements has an opening at the center. Because the present investigation shows the effectiveness of the center opening on the drag reduction for a curved model, the latter model is likely to produce less drag force than the former. This effect is expected to be notable for a large curvature model made of a small number of plates, and, in this case, the drag coefficient may be found to depend significantly on the number of plate elements.

Further systematic investigations, however, will be necessary in order to understand fully the effect of the geometry on the aerodynamic characteristics of the two-dimensional model. The present investigation should also be extended to include axisymmetric models as well as the effects of compressibility and Reynolds number.

Conclusions

Aerodynamic characteristics of two-dimensional slotted bluff bodies simulating ribbon parachutes were investigated

experimentally. Effects of spacing ratio (i.e., geometric porosity), curvature, and vent were analyzed.

Small-spacing ratio configurations ($s/h=0.25$) produced more stable near-wake formations than large-spacing ratio models ($s/h=0.5$). At the same time, vortex sheddings were enhanced by the smaller-spacing ratio.

Curvature of the slotted models was found to reduce the drag force considerably. As the model curvature was increased, wake boundary motion was reduced as a result of weakened vortex sheddings, and shedding frequency decreased, corresponding to a narrower wake. More symmetric and also stable near-wake patterns resulted from the larger model curvature.

Vent jet from the large curvature models ($H/W=0.5$) suppressed the vortex sheddings. On the other hand, center jets from the vent of the small curvature and flat-model configurations ($H/W=0.25$ and 0, respectively) were, in most cases, deflected substantially and produced highly asymmetric overall wake patterns. In particular, the vent combined with the large model curvature produced lower drag values than other models with the equivalent porosity.

Acknowledgment

This research was supported by Sandia National Laboratories Grant 33-8579.

References

[1]Spahr, H. R. and Wolf, D. F., "Theoretical Analysis of Wake-Induced Parachute Collapse," *Proceedings of the AIAA 7th Aerodynamic Decelerator and Balloon Technology Conference*, AIAA, New York, Oct. 1981.

[2]Blevins, R. D., "Flow-Induced Vibration," *Instabilities of Tube Rows and Arrays*, Van Nostrand Reinhold, New York, 1977, Chap. 5.

[3]Hayashi, M., Sakurai, A., and Ohta, Y., "Wake Interference of a Row of Normal Flat Plates Arranged Side by Side in a Uniform Flow," *Journal of Fluid Mechanics*, Vol. 164, March 1986, pp. 1–25.

[4]Higuchi, H., "Experimental Investigation of the Flowfield Behind Grid Models," *Journal of Aircraft*, Vol. 26, April 1989, pp. 308–314.

[5]Ball, D. J. and Cox, N. J., "Hydrodynamic Drag Forces on Groups of Flat Plates," *Journal of the Waterway Port Coastal and Ocean Division, Proceedings of the American Society of Civil Engineer*, Vol. 104, May 1978, pp. 163–173.

[6]Bearman, P. W. and Wadcock, A. J., "The Interaction Between a Pair of Circular Cylinders Normal to a Stream," *Journal of Fluid Mechanics*, Vol. 61, Part 3, Nov. 1973, pp. 499–511.

[7]Williamson, C. H. K., "Evolution of a Single Wake Behind a Pair of Bluff Bodies," *Journal of Fluid Mechanics*, Vol. 159, Oct. 1985, pp. 1–18.

[8]Hayashi, M., Sakurai, A., Aso, S., and Tenhiro, S., "On the Aerodynamic Characteristics of Two- and Three-Dimensional Concave Bodies," *Technology Report of the Kyushu University*, Vol. 57, March 1984, pp. 137–142 (in Japanese).

[9]Hayashi, M., Aso, S., Tenhiro, S., and Nakaya, H., "Drag of the Fundamental Shapes of Parachutes," *Technology Report of the Kyushu University*, Vol. 57, Aug. 1984, pp. 463–470 (in Japanese).

[10]Roberts, B. W., "Drag and Pressure Distribution on a Family of Porous, Slotted Disks," *Journal of Aircraft*, Vol. 17, June 1980, pp. 393–401.

[11]Takahashi, F., "Aerodynamics of Two-Dimensional Slotted Bluff Bodies," M.S. Thesis, Univ. of Minnesota, April 1988; also Sandia Albuquerque, NM, Rept. SAND 88-7151, April 1988.

[12]Stock, D. E., Wells, M. R., Barriga, A., and Crowe, C. T., "Application of Split-Film Anemometry to Low-Speed Flows with High Turbulence Intensity and Recirculation as Found in Electrostatic Precipitators, *Proceedings of the 5th Biennial Symposium on Turbulence*, University of Missouri, Rolla, 1977, pp. 117–123.

[13]Allen, J. H. and Vincenti, G. W., "Wall Interference in a Two-Dimensional Flow Wind Tunnel, with Consideration of the Effect of Compressibility," NACA Rept. 782, 1944.

[14]Castro, I. P., "Wake Characteristics of Two-Dimensional Perforated Plates Normal to an Air Stream," *Journal of Fluid Mechanics*, Vol. 46, Part 3, 1971, pp. 599–609.